Universiteit Utrecht

Faculteit Bètawetenschappen

A search for an atomically flat Pb surface and an outlook on CO manipulation on Pb

Bachelor Thesis

Meike Bos

Natuur- en Sterrenkunde

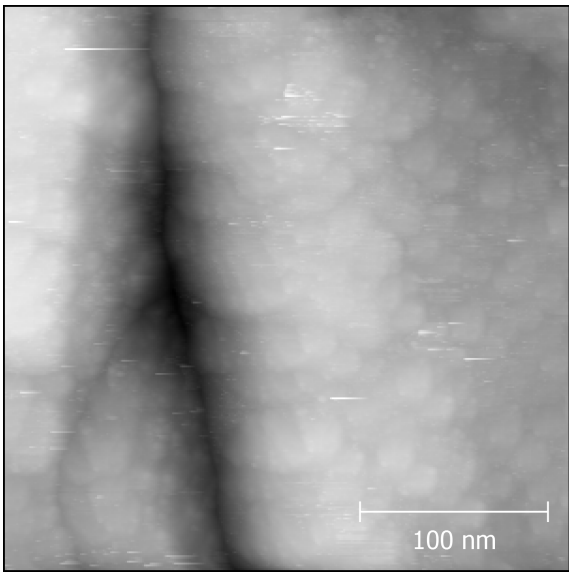

Supervisors:

Dr. I. Swart Supervisor
Debye Institute

S.E. Freeney MSc Daily Supervisor
Debye Institute

June 14, 2017

Abstract

Scanning tunnelling microscopy can be used to study metal surfaces on an atomic level. An interesting metal to study is lead because it is superconducting below 7.2 K. With a scanning tunnelling microscope single molecules like CO can be manipulated to build artificial structures. These structures confine the electrons and hence give rise to specific energy bands. Before measurements can be done the metal surface has to be atomically flat. The creation of atomically flat Pb(111) and Pb(100) was attempted using etching, sputtering and annealing. Atomically flat lead surfaces were not yet obtained. An outlook on the possibility of manipulating CO on Pb(111) is explored using density functional theory calculations. The results were compared with density functional theory calculations of CO on Au(111) and CO on Cu(111). The CO does not bind directly above an Pb atom at the surface, but does bind in both bridge- and three-fold hollow sites of the Pb surface. The calculated binding energies are comparable to the binding energy of CO on Cu(111). This suggests that atomic scale manipulation of CO on Pb is possible.

Contents

1 Introduction

In scanning tunnelling microscopy (STM) an atomically sharp tip is brought close to a conducting surface, a tunnelling current is used to image electrical changes on the surface. This allows for atomic resolution. A scanning tunnelling microscope can manipulate single atoms or molecules on the atomic scale. This has been used to build artificial structures with interesting energy bands, like artificial graphene[1] and a lieb lattice[2]. Using artificial lattices energy band structures can be obtained which are not seen in nature. For example the lieb lattices gives rise to a dirac cone with a flat band trough it[2]. Lead is known to be a superconductor at temperatures below 7.2 K[3]. The low temperature microscope used in this project is cooled with liquid helium to a temperature of 4.5K. This makes it possible to do measurements with the microscope on superconducting surface states. However before this is possible it is necessary to obtain atomically flat Pb surfaces. S. Speller et all. (1995) obtained atomically flat Pb(111) and Pb(110) surfaces using etching and cycles of sputtering with argon and annealing. They looked to the movement of step edges on the surface at room temperature[4]. M. Ruby et all. (2015) obtained atomically flat Pb(111), Pb(110) and Pb(100) surfaces using cycles of sputtering with Neon and annealing to 430 K[3]. They measured the structure of the superconducting gap for the different lead surfaces. In this thesis obtaining atomically flat Pb surfaces is the main goal. The surfaces used are Pb(111) and Pb(100). We also want to determine if it is possible to do CO manipulation on a Pb(111) surface. This is done using density functional theory (DFT) calculations. The outcomes are compared to CO on Cu(111) calculations and literature and CO on Au(111) calculations and measurements with the low temperature STM. Fistly the theory of the STM will be explained, and subsequently properties of the lead sample, CO manipulation, the Cu(111) and the Au(111) surfaces and density functional theory calculations. In the methods section the different techniques used to clean the sample are explained: etching, sputtering and annealing. An overview is given for the steps taken for each sample. Finaly the DFT calculations are explained.

2 Theory

2.1 Scanning Tunnelling Microscopy (STM)

STM is possible because of the existence of a tunnelling current between the tip and the sample when the Fermi levels of the tip and the sample are not equal. The vacuum between the tip and the sample is a potential barrier. In the tip and the sample the Schrödinger equation allows for free waves below their Fermi energies. The mean barrier height can be expressed in terms of the work functions of the tip and the sample. The work function ϕ of a surface is defined as the difference between the Fermi energy and the energy of the vacuum (see figure 1(a)). The sample and the tip are in electrical contact so their Fermi levels are aligned (if there is no bias voltage, see figure 1(b)). However the work functions stay the same, so the effective energy of the vacuum is different for the tip and the sample. Due to the applied bias voltage V the Fermi level of the tip and the sample differs by eV, where e is the elementary charge (see figure 1(c)). For a positive bias voltage the Fermi energy of the sample is eV lower than the Fermi energy of the tip. The electrons can only tunnel in this eV window, so for a positive bias voltage they can only tunnel from the tip to the sample. This gives a tunnelling current from the sample to the tip. For a negative bias voltage the electrons tunnel from the sample to the tip. This gives a tunnelling current from the tip to the sample. The mean height of the potential barrier can be approximated as the mean of the work function of the tip and the work function of the sample. The difference between the energy of the barrier and the energy ϵ at which the electrons tunnel is given by (with ϵ between 0 and eV):

$$\frac{\phi_{tip} + \phi_{sample}}{2} + \frac{eV}{2} - \epsilon$$

Using this results in the the transmission factor, given by[1]:

$$T(\epsilon, V, z) \propto e^{-2z\sqrt{\frac{2m_e}{\hbar^2}\left(\frac{\phi_{tip}+\phi_{sample}}{2}+\frac{eV}{2}-\epsilon\right)}} \tag{1}$$

[1]See B.Voigtländer: Scanning probe microscopy[5] chapter 20 for more details on the transmission factor

With m_e the mass of the electron. The current is proportional to the transmission factor. It can be seen that the current decreases exponentially with increasing tip sample distance z and decreases with increasing bias voltage V.[5]

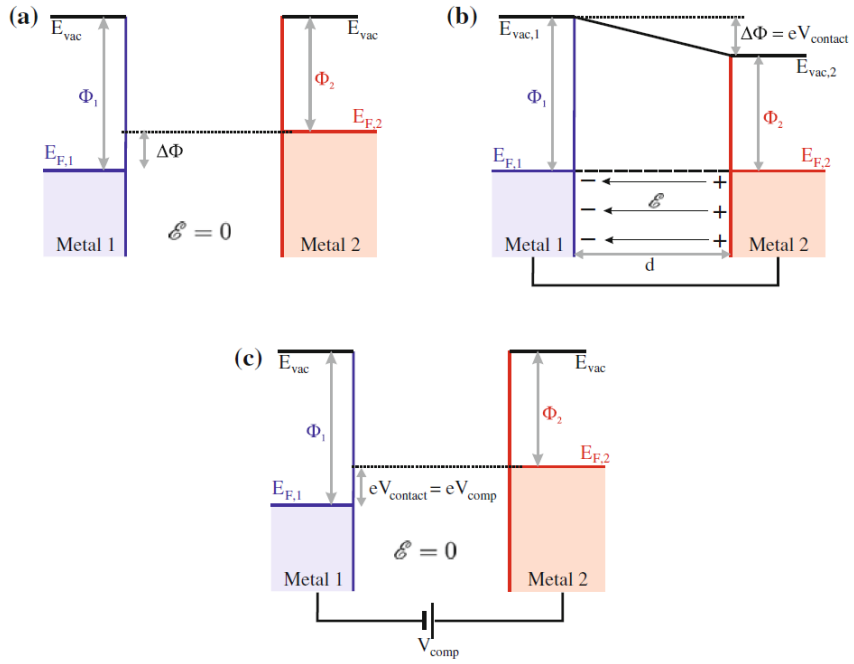

Figure 1: Potential energy diagram for two metals (a) not connected (b) connected without bias voltage applied (c) connected with bias voltage V applied.[5]

2.1.1 Tip Movement

For scanning the surface of the sample it is necessary to move the tip with picometer accuracy. This is possible due to the piezoelectric elements attached to the tip. Piezoelectric materials change their shape depending on the voltage applied. Piezoelectric materials have a permanent dipole. The applied voltage gives rise to an electric field in the piezoelectric material. The permanent dipole in the material changes its position in the energetically most favourable way. This will cause deformation of the material. A typical value for the piezoelectric constant is around 15 nm/V.[6] This means a voltage of 1 V has to be applied to move 15 nm. If the applied voltage is suddenly changed, the piezoelectric elements need time to adjust. This gives the effect that the image seems to shift when the scan is started immediately after moving e.g. straight lines appear to be bent. This effect is named creep. To avoid creep while scanning each line has to be scanned forwards and backwards before going to the next line, for a jump to the next line will cause a deformation of the image. After moving a larger distance to scan another area the creep will disappear after some time.[5]

2.1.2 Topograph of the Sample

To obtain an image of the sample, named a topograph, the STM either measures with constant current or at constant height.
In constant height mode the tip scans at a certain z position over the surface. The current is measured. The sample is often tilted with respect to the tip and the surface has step edges. Because of this the separation between the tip and sample does not remain constant. There is a chance of crashing the tip into the sample in this mode.
The constant current mode is more often used. In constant current mode the current between the sample and tip is kept constant. This is done using a feedback loop. The feedback loop consists of a combination of a proportional controller and a integral controller (PI-controller).

The proportional controller gives a feedback proportional to the error measured between the pre-set value and the measured value. The output y is given by the following formula:

$$y = K_p(w - x) \tag{2}$$

Where w is the pre-set value, x is the measured value and K_p is the proportional gain. How fast this feedback works is dependent on the magnitude of the proportional gain. The larger the proportional gain the faster the feedback system, however the larger the feedback gain the larger the overshoot. There are different ways how the output y can change the measured value x. One of the options is that the value of x simply changes into the value of y, but other more complex relations are also possible. The proportional controller has a steady-state error. For example when the output y simply changes x by replacing its value with the value of y the solution for the steady state situation $K_p(w - x) = x$ is given by $x = \frac{wK_p}{1+K_P}$. It follows that $w \neq x$ for $w \neq 0$. Even when the output y changes the measured value x in a different way a steady state error remains. The steady state error is proportional to $1/K_p$.
The integral controller can be used to correct for the steady state error of the proportional controller. The output of the controller is given by:

$$y(t) = K_l \int_{t_1}^{t_2} (w - x(\tau))d\tau \tag{3}$$

where w is the pre-set value, $x(\tau)$ is the measured value and K_l is the integral gain.[5]

If the sample is tilted with respect to the tip, a slope is measured which can be a lot bigger than the differences in height of structures on the surface. A background subtraction can be done after measuring with an image processing programme to subtract the slope of the sample from to image, so the structures on the surface are more easily seen.[5]

2.2 Lead crystals

Lead has a face centred cubic crystal structure with a monatomic basis. There are different kinds of surfaces for lead crystals, depending on how the surface is cut. We used two crystals with different surface orientations given by the Miller indices (111) and (100). These crystals will be addressed as Pb(111) and Pb(100) respectively.

2.2.1 Surface State of Lead

Metal single crystals can support a so-called electronic surface state. The wave function of this state has a peak at the surface and decays exponentially into the vacuum and into the bulk. Hence, electrons in these states are confined in the plane of the surface and form a 2D electron gas.[7] These states can be imaged with an STM.[5]
STM can be used to measure the surface states of a crystal. However the crystal also has bulk states. In perfect crystals the surface states are orthogonal to the bulk states. Due to defects on the surface the electrons in the surface state can scatter to the bulk state. These defects can be anything from adatoms to step edges. The scattering of the electrons causes broadening of the line width of the measured energy levels.[8]

It has been shown that at room temperature the step edges on the surfaces of Pb(111) and Pb(110) crystals move around in a time frame it takes to make an overview scan of the surface at constant current. This causes step edges to appear frizzy (see figure 2). It was found that the step edge speed is faster than 0.5 nm/s and that a single atom hops at most once in a time frame of 3 ms.[4].

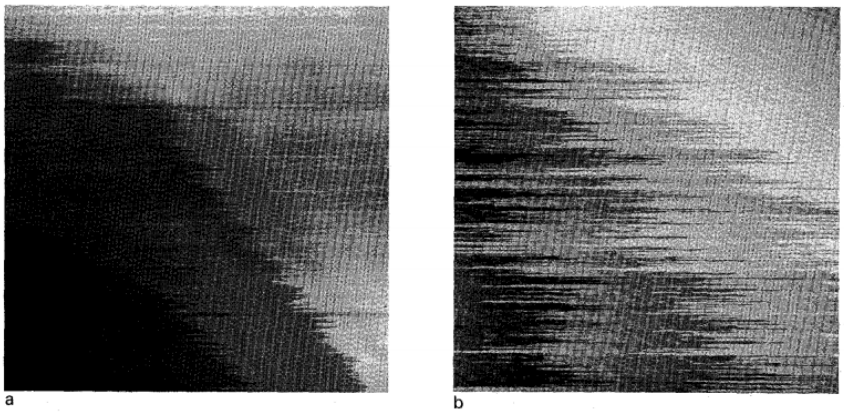

Figure 2: Results from S.Speller et al. (1995)[4] (a) topograph of Pb(111) (b) topograph of Pb(110), $V_t = -0.4$ V, $I_t = 1.3$ nA.

2.2.2 Superconductivity of Lead

Lead is a type 1 superconductor at temperatures below 7.2 K[3]. An effect seen in superconductors is the Meissner effect which is where an external magnetic field is excluded from the superconductor. This is due to induced electric currents causing an magnetic field in the superconductor equal in magnitude and opposite to the applied magnetic field. The field is not completely excluded from the superconductor for finite temperature. How deep the magnetic field penetrates the superconductor is dependent on the temperature. This can be explained by the fact that the density of superconducting electrons increases with decreasing temperature. Superconductor electrons are electrons that form Cooper pairs. When all electrons are bound as Cooper pairs the energy needed to brake one Cooper pair is the highest. This causes the superconducting energy gap. If the temperature is non zero thermal excitations cause some pairs to break. This causes the energy gap to decrease. With increasing temperature it becomes easier to break Cooper pairs, till there are no cooper pairs left at the critical temperature.[9]

2.3 Manipulation of Single Atoms with the STM

Single atoms or molecules can be adsorbed onto the sample surface. This can be metal atoms (e.g. Cu, Pb) or molecules (e.g. CO).[10] These adsorbates can be moved to a preferred position with the use of the STM tip. There are two types of manipulations: Vertical manipulation (see figure 3(b)) and lateral manipulation (see figure 3(a)). For both types of manipulations it starts with moving the tip above the adsorbate.Then the height in z is reduced and if necessary a voltage pulse is applied. In vertical manipulation the settings are changed in such way that the chemical bond between the surface and the adsorbate is broken and the adsorbate jumps to the apex of the tip. After this the tip is moved to the desired lateral position and the tip is brought close to the surface again and the reversed voltage is applied. This voltage pulse breaks the bond between the adsorbate and the tip and the adsorbate sits on the surface again. In lateral manipulation the tip is moved closer to the surface so that the adsorbate forms a bond with the tip and the surface simultaneously. Then the adsorbate is dragged to the desired lateral position where the bond between the tip and the adsorbate is broken.[11]

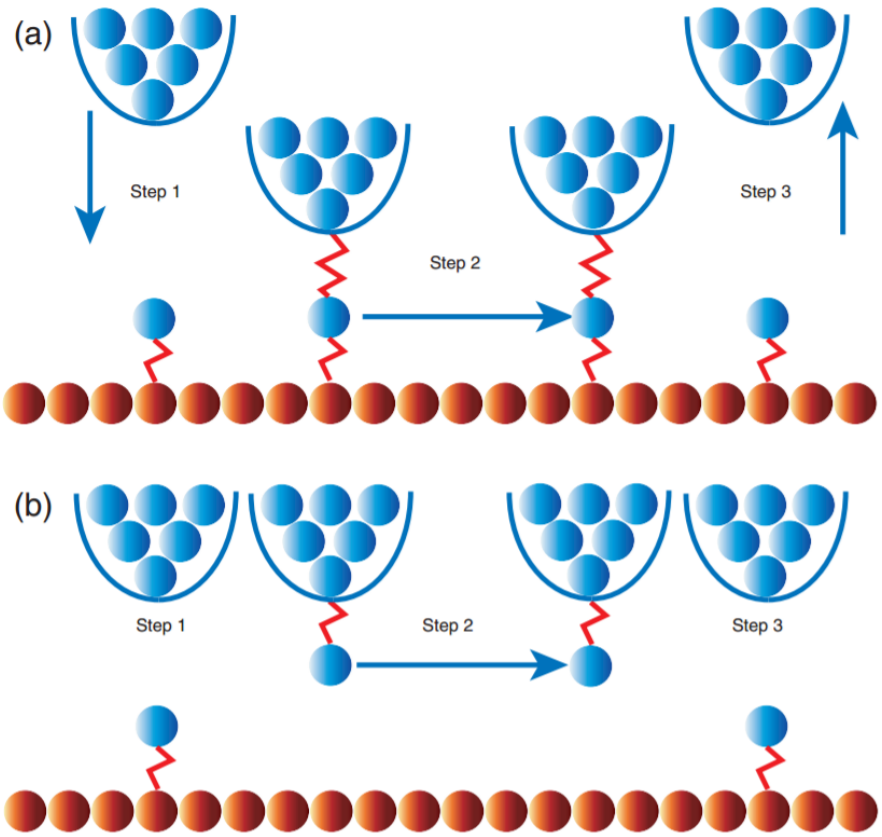

Figure 3: Schematic overview of (a) lateral manipulation with in STM (b) vertical manipulation in STM. The circles represent atoms and the red lines represent chemical bonds.[11]

2.4 Cu(111) surface

CO molecules can be manipulated with an STM at low temperatures on the surface of a Cu(111) crystal[12][13]. The CO is absorbed directly ontop of a Cu atom. CO on a copper surface appears like a depression with a metal tip.[13]

2.5 Au(111) surface

The Au(111) surface has been studied under a low temperature STM. The surface of Au(111) reconstructs. It forms parts with an fcc structure and part with a hexagonal close packed (hcp) structure. This shows under a scanning tunnelling microscope as herringbones. An example of these herringbones under a microscope is shown in figure 4. The small area between two light lines has a hcp structure while the wide area has an fcc structure.[14]

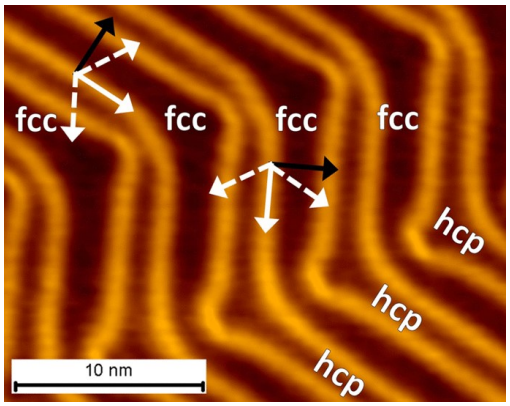

Figure 4: Picture from C.J.Murphy et all.(2015)[15]. Shown is the surface of Au(111) under a scanning tunnelling microscope. Temperature: 78K, bias voltage: 300mV, current: 200pA. The parts with hcp and fcc structure are labelled.

2.6 Density Functional Theory

To investigate how CO absorbs onto a Pb(111) surface density functional theory (DFT) was used. Solving the Schrödinger equation exactly for a system consisting of multiple atoms with multiple electrons is not possible. Approximations have to be made to obtain information about the system. In DFT the wave equations are replaced by the electron density. It has been shown that the Hamilton operator is uniquely determined by the electron density[16], so it is possible to use the electron density to find all the properties of the system. Parts of the potential are approximated and the problem is solved numerically. Many properties of a system can be determined using DFT. For example the geometry of a certain system can be optimised (by minimizing the energy),the corresponding lowest energy value can be found and a spatial distribution of the electron density can be calculated.[17]
A more detailed introduction of density functional theory is beyond the scope of this thesis. The interested reader can find more information in the book of M.C.H. Wolfram Koch: A Chemist's Guide to Density Functional Theory[17].

3 Method

3.1 Experimental Set-up

The set-up consists of two microscopes, a preparation chamber and a load lock, see figure 5. The microscopes are called the Fermi microscope, this is a scanning tunnelling microscope at room temperature, -and the low temperature (LT) microscope,- this is a scanning tunnelling microscope operating at 4.5K. The set-up is under ultra high vacuum (base pressure $< 5 \times 10^{-10}$ mbar) with all parts connected, so when a sample is moved from one part of the set-up to another part it does not leave the vacuum. A close up of the preparation chamber and load lock is shown in figure 6.

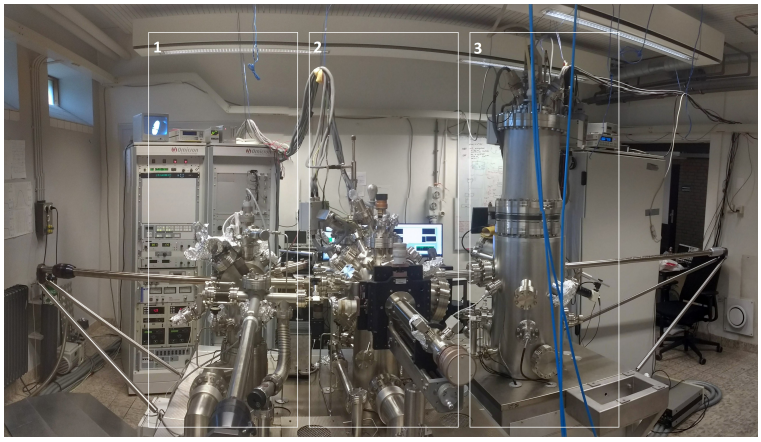

Figure 5: A overview picture of the total set-up. Window 1 contains the preparation chamber and the load lock, window 2 contains the Fermi microscope and window 3 contains the low temperature microscope.

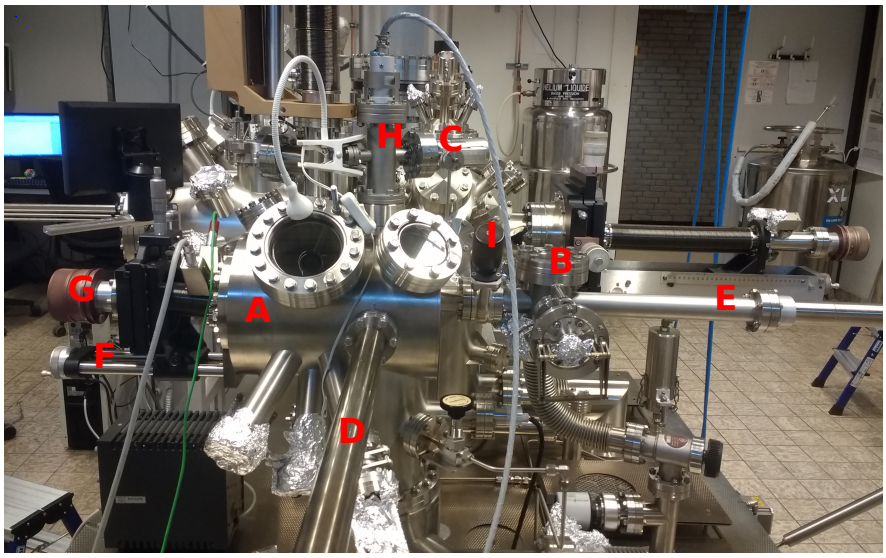

Figure 6: A picture of the preparation chamber and the load lock with parts labelled A: Preparation chamber, B: Load lock, C: Valve for argon leakage, D: Arm from preparation chamber to Fermi microscope, E: Manipulation arm from load lock to preparation chamber, F: Heater arm preparation chamber, G: Knob to rotate heater arm preparation chamber, I: Valve between load lock and preparation chamber, H: Ion gun.

3.2 Preparation of the Sample

There were two lead samples with different surfaces used. Pb(111) made a few years ago (bar shaped) and Pb(100) made in 2017 (circular shaped).

3.2.1 Cleaning of Sample outside the vacuum

The samples were delivered in a sealed casing. The sample plates were cleaned with ethanol and acetone. The oxygen layer of each sample was etched away by submerging it into a solution of ca. 20 ml acetic acid with a few drops of hydrogen peroxide (concentration: 30% by weight). Afterwards it was cleaned with pure acetone. The samples were put onto their sample plates and placed in the set-up under ultra-high vacuum.

3.2.2 Sputtering and Annealing

An atomically clean surface can be obtained by the process of sputtering and annealing. This happens in the preparation chamber (figure 5 number 1).
Sputtering is a process in which contaminants and a few monolayers are removed from the sample by bombarding the sample with accelerated argon ions. The argon used has a concentration of 99.99% and is made by The Linde Group. Because argon is a noble gas it does not react with the surface. So sputtering is a a completely mechanical process. Sputtering is done using the following steps:

- The sample is placed in the preparation chamber, positioned under the ion gun (letter H figure 6) under ultra high vacuum. Argon gas is leaked in until the pressure is around 4×10^{-6} mbar.
- The argon gas is ionised by electrons with a current of 10 mA.
- The argon ions are accelerated to the sample by applying a high voltage between the filament and a plate below the sample.
- This process is continued for a certain amount of time.

Depending on the settings used the profile of the pressure of the argon ions is different. We aim for an evenly distributed profile over the entire sample. We therefore use the following settings:
Energy: 1kV
Extractor: 517V
Focus: 811V.
The settings were changed one time during sputtering in this project to a more focused setting (see Appendix A table 2):
Energy: 5Kv
Extractor 4410V
Focus 4143
Sputtering leaves a disordered surface. In annealing the sample is heated in order to make the surface of the sample reconfigure to a more ordered state. Annealing consists of the followings steps:

- The system is set to resistive heating so that a current can flow trough a tungsten wire below the sample plate.
- The current is set to the desired value (see figure 7). As can been seen in the figure the reaction of the temperature is not instant but will increase over time until it reaches an end value. This takes 5 to 15 minutes. For the lead samples an annealing temperature of 400 to 450 K is used in literature.[18][19][20][3].
- Anneal for a certain time so the surface is flattened.

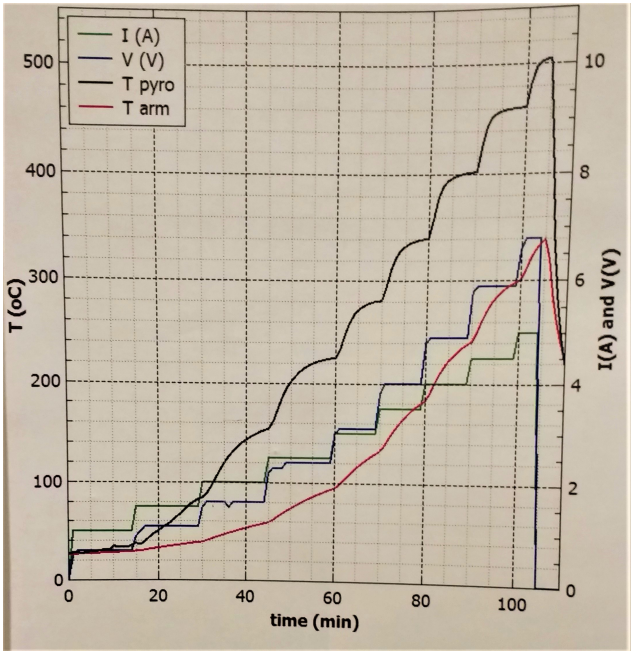

Figure 7: Calibration preparation heater arm 15 minutes at each current.

Several rounds of sputtering and annealing are needed to clean the surface. During annealing defects that are just below the surface can diffuse to the surface. These defects have to be sputtered off. The sample can also be sputtered warm. In this case, the same steps as during sputtering are followed and in addition to this the sample is heated in the same way as it is during annealing. The temperature for warm sputtering is lower than the temperature used in annealing.

3.2.3 Preparation of Pb(111)

The Pb(111) crystal was first put into the set-up without etching. In table 2 in Appendix A an overview is given of the sputtering and annealing cycles of the un-etched Pb(111).
After this the sample was taken out of the vacuum again and etched for 1 hour and 31 minutes. See figure 20 in Appendix A for picture of the sample before and after 5 minutes of etching. During etching the sample changed colour: it started at white grey and was not shiny(see left picture appendix), at the end it was shiny silver grey (see middle of the bar right picture appendix). The sample reduced in size, the edges where rounded and the height of the crystal decreased by several micrometers. The sample was put into the vacuum, via the load lock, less than 30 minutes after it had been etched.
The sample was sputtered and annealed. In table 3 in Appendix A an overview is given of the sputtering and annealing cycles.

3.2.4 Preparation of Pb(100)

The sample was etched for 11 minutes. Before etching the sample had a dark grey colour and was not shiny. The surface consisted of two different shades of grey. Within the first few seconds the sample became shiny. The surface consisted still of two different shades of grey. See figure 21 in Appendix B for picture of sample directly after etching. After etching the sample was secured onto the sample plate and put into the vacuum, via the load lock, in less than 30 minutes after etching. The sample was sputtered and annealed. In table 4 in Appendix B an overview is given of the sputtering and annealing cycles. After sputtering and annealing the dark spot became more pronounced (see figure 22 in Appendix B).

3.3 Measurement with the scanning tunnelling microscope

We used two different scanning tunnelling microscopes. A microscope at room temperature that is called the Fermi microscope (see window 2 figure 5) and a low temperature (LT) scanning tunnelling microscope that operates at a temperature of 4.5 K. The LT microscope is cooled using liquid nitrogen and liquid helium. For measurement with the STM the software MATRIX 3.2 is used.

3.3.1 Approaching the Sample for Measurement

To reduce noise from the surrounding the sample and tip in the Fermi microscope and the LT microscope are hanging in springs. For the LT microscope active vibration damping is used next to this. When everything is set the tip has to approach a desired position on the surface. If the tip is far away the tip is brought closer first by moving the tip closer mechanically with course steps. This is done by a user while looking at the camera image. When the tip and the sample are close the option auto approach is used. The loop gain is set to 15% or 20%. When a current is detected, the tip stops approaching. When the tip has auto approached the loop gain is set back to a value between 3% and 7% and the piëzo position is set to (0,0). A scan can be initiated.

3.3.2 Tip Preparation

For good measurements with the scanning tunnelling microscope a stable atomically sharp tip has to be made. This can be done by tip preparation. Tip preparation is a process of trial and error. The tip can be conditioned using the following options:

- Voltage Pulse: A Voltage pulse is applied. This magnitude of the pulse can be controlled. The lowest value used is around 1 V. The highest value used is around 10 V.
- Z-ramp: The tip is quickly moved into the surface and moved away again. The idea is that the tip crashes into the surface. In this way the tip can leave atoms on the surface and pick atoms from the surface. It can be set how much closer it moves than its current position. The value at which the tip touches the sample depends on the applied current and voltage bias. The minimum value is used around -0.5 nm.

A Z-ramp and a voltage pulse can also be combined during tip preparation.
After applying a voltage pulse or a Z-ramp the tip is moved away from the current scanning position because dirt on the sample can change the tip. The following problems can be encountered during tip preparation:

- Unstable tip: The tip is unstable and this gives a blurry image. To make te tip stable again a voltage pulse or a Z-ramp can be applied.
- Dragging something along the tip: If dirt on the sample is to high in $z$or the tip is too close, sometimes adsorbates are dragged along with the tip. This can be solved by using a voltage pulse and moving to another scanning position.
- Multiple tips: The tip has multiple apices so characteristics on the surface show up multiple times. This can be solved by using a Z-ramp.

A good tip is stable for multiple currents and sample biases.

3.3.3 Measurement of CO on Au(111)

The Au(111) was cleaned by sputtering and annealing the sample. The Au(111) was placed in the LT-microscope, it was checked to see if the surface was clean enough. After this the tip was retracted and CO was leaked in. It was leaked in at a pressure of 1.2×10^{-8} mbar for 5 minutes. The tip was approached again and the measurement of CO on Au(111) was initiated. Different bias voltages and currents were used.

3.4 DFT calculation

DFT calculations were used to find the optimum geometry, the change in the final total energy and change in the spatial distribution of the electron density after adsorption of CO. The systems investigated with the calculations are a CO molecule above different metal surfaces. The surfaces used here are Pb(111), Au(111) and Cu(111).The calculated values can differ from the real values. Trends in the calculated values are less delicate and hence the calculated values for CO on Au(111) and CO on Cu(111) are used as benchmark for the calculated values for CO on Pb(111). It has been shown that CO absorbs directly on top of a metal atom for Cu(111) and Au(111)[21]. For Cu(111), Au(111) and one configuration of Pb(111) the CO is placed directly above a metal atom with the carbon atom directly above the metal atom and the oxygen atom directly above the carbon atom. This site of the CO will be referred as top site. The surface is represented by the metal atom right below the CO and all its nearest neighbours. For example the Au(111) surface with CO on top is plotted in figure 8. The program ORCA 4.0[22] was used for the DFT calculations.

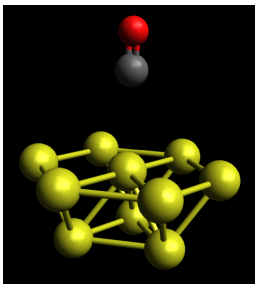

Figure 8: Picture of configuration of Au(111) surface with CO on top plotted in Avogadro (molecule editor and visualiser program)[23], the same configuration is used for the Cu(111) with CO system and one of the Pb(111) with CO systems.

For the Pb(111) two additional configurations were also used. For the first the carbon atom is placed directly above the spot between three lead atoms and the oxygen atom is placed directly above the carbon atom. This site is named three-fold hollow site. One Pb atom of the second layer (directly under the carbon atom) is taken into account. See figure 9 for a plot of this configuration.
The other configuration is the carbon atom directly above the spot between two lead atoms. The oxygen atom is placed directly above the carbon atom. Two-fold hollow site is used to refer to this site. Two extra lead atoms closest to the two Pb atoms are added and two of the nearest atoms from the second layer. See figure 10 for a plot of this configuration.

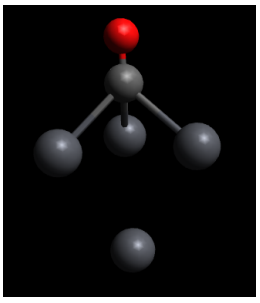

Figure 9: Picture made with Avogadro[23] of configuration of Pb(111) with CO placed on the three-fold hollow side of Pb(111).

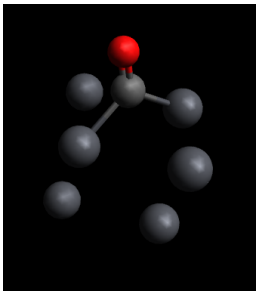

Figure 10: Picture made with Avogadro[23] of configuration of Pb(111) with CO placed on the two-fold hollow side of Pb(111).

3.4.1 Geometry Optimization

For the geometry optimization the positions of all the metal atoms were fixed such that the distances between the metal atoms match those in a bulk crystal[24]. The CO atom was constrained so it was only possible to move vertically above the surface but not horizontally. The Perdew–Burke–Ernzerhof exchange-correlation functional was used. Furthermore the options SLowConv and NOSOSCF were used and a TZVP basis set was used. ORCA first optimizes the geometry. When this has converged ORCA calculates the final total energy of the system. The final coordinates can be read in the .XYZ file generated by ORCA.

3.4.2 Change in Final Total Energy

The geometry optimization described above gives the final total energy of the system in eV. The change in energy between the CO on the metal surface and the CO molecule and the metal surface separate was calculated. This was done by running an ORCA calculation for the CO molecule separate (without any constrains) and an ORCA calculation for the metal surface (with all positions constrained). The obtained final energies are subtracted from the final energy found for the total system and this gives a measure for the strength of the binding energy of the CO the the metal surface.

3.4.3 Change in electron density

The final geometries and energies calculated are used to calculate the spatial distribution of the electron density of the system. The range chosen is from -20 Bohr to 20 Bohr in the x, y and z direction with a grid of 80 by 80 by 80. This is done for the total system of the metal and the CO. The information about the electron density is found in a .cube file generated by ORCA. A second .cube file is generated with only CO fixed at the same coordinates as found in the geometry optimization. A third cube file is generated with only the metal atoms fixed at the same position as in the geometry optimization.
The cube file of the CO separated and the cube file of the metal only are subtracted from the cube file of the total system using a python script. This gives a cube file with the change in electron distribution due to the binding energy of the CO to the metal. This is plotted using Avogadro[23].

4 Results and Discussion

4.1 STM Measurements

4.1.1 Pb(111) Measurements

The measurements of Pb(111) are viewed in chronological order. See table 2 and 3 in Appendix A for information on sputtering and annealing cycles.

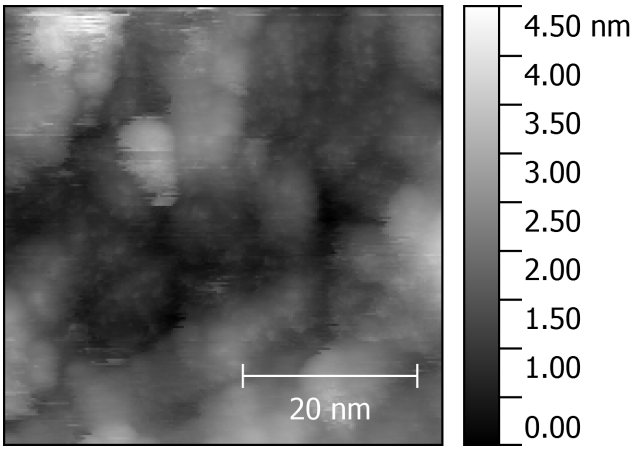

Figure 11: 50x50 nm overview scan in constant current mode of surface Pb(111) made at room temperature (Fermi microscope). Settings: current: 0.05nA, voltage bias: 1.0V, loop gain: 8%, number of points: 200, number of lines: 200.

In figure 11 it can be seen that the surface is not atomically flat. No step edges or flat areas can be seen. There are dome shaped areas with a diameter varying between 5 nm and 10 nm.

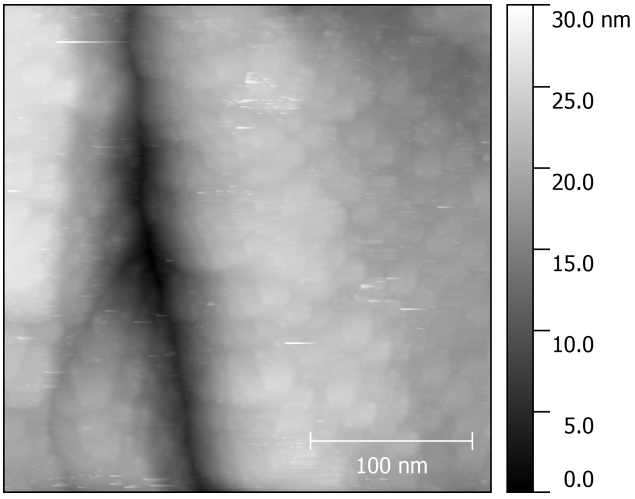

Figure 12: 250x250 nm overview scan in constant current mode of etched surface Pb(111) made at room temperature (Fermi microscope). Settings: current: 0.02nA, voltage bias: 1.0V, loop gain: 3%, number of points: 300, number of lines: 300.

In figure 12 the surface is not atomically flat and no step edges can be seen. The surface has the same general shape as in figure 11.

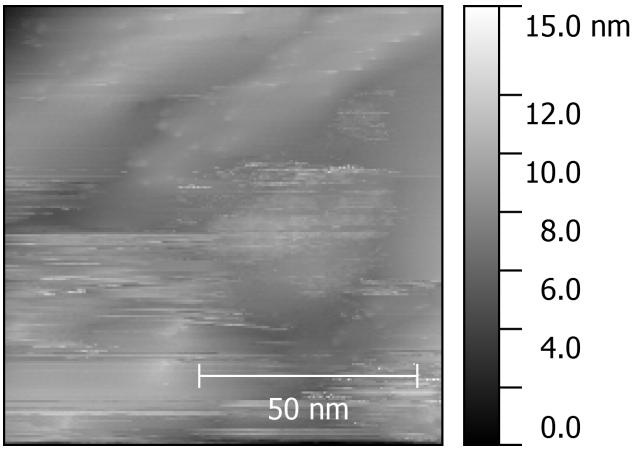

Figure 13: 100x100 nm overview scan in constant current mode of surface Pb(111) made at room temperature (Fermi microscope). Settings: current: 0.3 nA, voltage bias: 1.0 V, loop gain: 4%, number of points: 200, number of lines: 200.

In figure 13 it can be seen that the surface of the Pb(111) is not atomically flat over large areas. However it looks different than it did before in figures 12 and 11. The small dome shaped height differences on a scale of 10 nm are gone. This makes the overall shape more flat than before. To make an atomically flat surface an higher annealing temperature could be used.

4.1.2 Pb(100) Measurements

The measurements of Pb(100) are viewed in chronological order. See table 4 in Appendix B for after how many sputtering and annealing cycles the measurements were taken. All measurements shown below are taken at the dark spot of the sample.

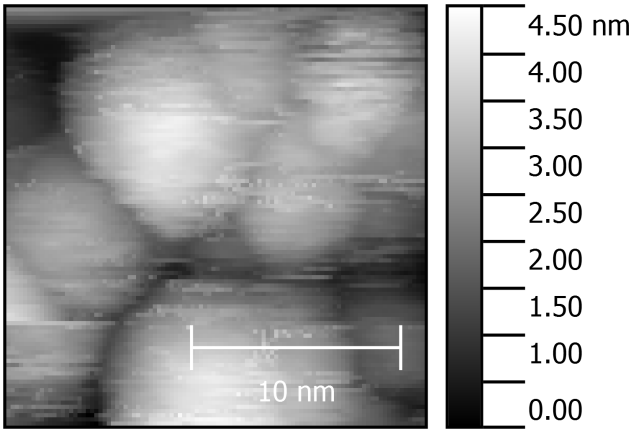

Figure 14: 15x15 nm overview scan in constant current mode of surface Pb(100) made at room temperature (Fermi microscope). Settings: current: 0.1nA, voltage bias: 2.6V, loop gain: 1.5%, number of points: 100, number of lines: 100.

In figure 14 it can be seen that the surface is not atomically flat. The general shape of the surface is the same as for the Pb(111) in figure 11 and 12.

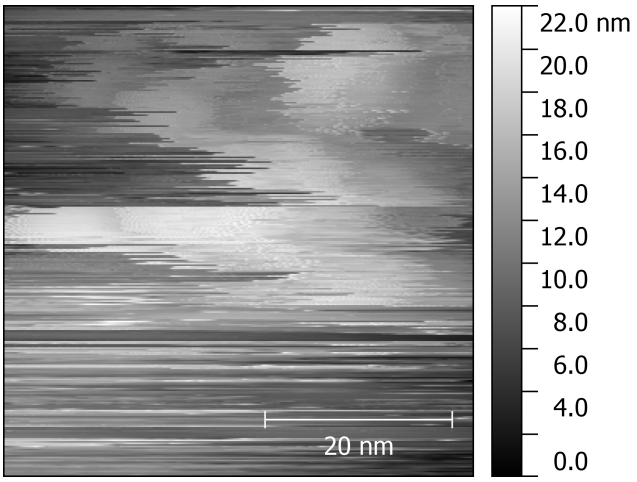

Figure 15: 50x50 nm overview scan in constant current mode of surface Pb(100) made at room temperature (Fermi microscope). Settings: current: 0.1nA, voltage bias: 1.0V, loop gain: 4%, number of points: 300, number of lines: 300.

In figure 15 it can be seen that the surface looks more flat than before. There seem to be some lines with the shape of step edges. However the height of these edges is too large for them to be step edges. Step edges with a height less than one nm are expected while the height difference observed here is of the size of a few nm.
In figure 16 a overview scan of Pb(100) in the LT microscope at 4.5K is shown. The noise is much less than under the Fermi microscope(figure 15) (a slower moving surface and a better isolated system). The surface is however not atomically flat. An option one has to make atomically flat surfaces in the future is annealing to a higher temperature.

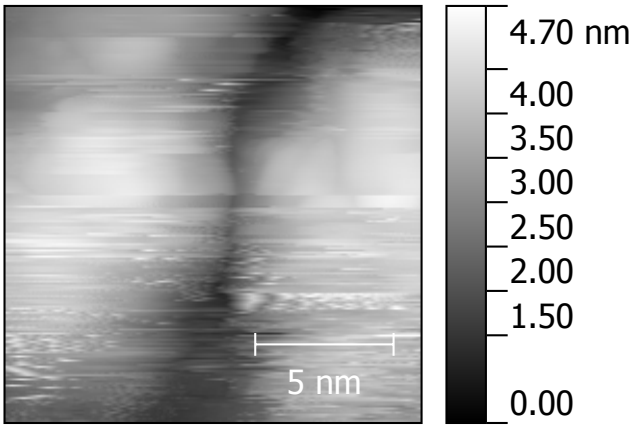

Figure 16: 20x20 nm overview scan in constant current mode of surface Pb(100) made at 4.5K (LT microscope). Settings: current: 0.1nA, voltage bias: 2.0V, loop gain: 5%, number of points: 200, number of lines: 200.

4.2 Au(111) Measurements

The CO was visible on the Au(111) as depressions, see figure 17. They look very similar to CO on copper. They attached to the fcc part of the gold atoms, also used in the DFT calculations. During scanning the CO molecules disappeared from the surface as can been seen in the figure. They most likely got adsorbed to the tip. As found in the DFT calculations (see below), the bindings-energy of CO on Au(111) is lower than CO on Cu(111). This is consistent with the observation that CO molecules are less mobile on Cu(111) than on

Au(111). This can explain why the CO molecules got picked up. Before the gold was put in the STM there were measurements done with other molecules and metals.

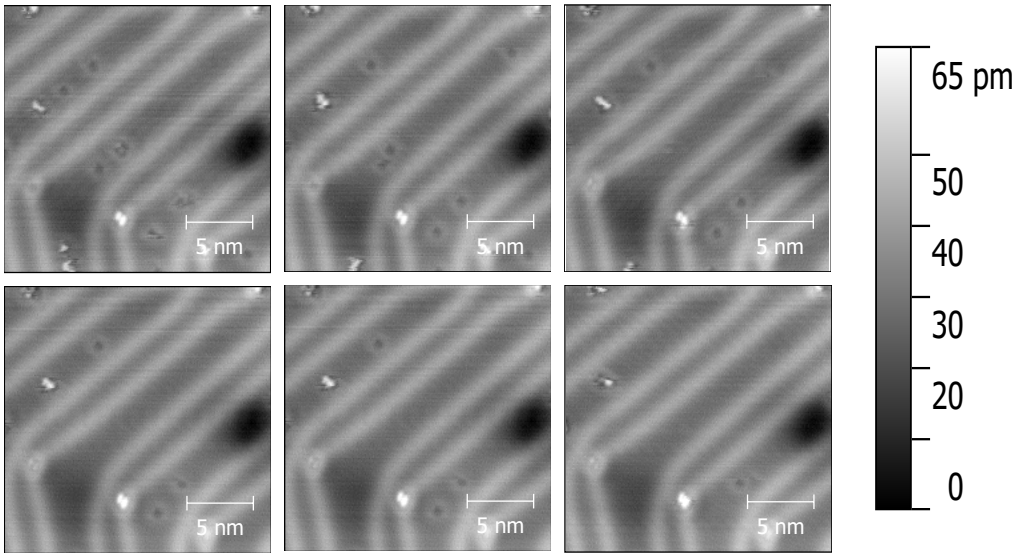

Figure 17: Succesive scans of 20x20nm in constant current mode of surface Au(111) with CO made at 4.5K (LT microscope). Pictures shown in chronological order from left to right. Settings: current: 0.01nA, voltage bias: 0.60V, loop gain: 7%, number of points: 200, number of lines: 300.

4.3 DFT Calculations

In table 1 the results for the geometry optimization and the change in total energy and are shown for the DFT calculations. As a reference the bindingsenergy of CO on a terrace of Cu(111) is shown[25]. It can be seen that the CO is the closest to the lead surface with the CO placed at the two-fold hollow site and the most far away for lead when the CO is placed on top. The difference in the final energies is comparable for gold and copper. For the Pb(111) it was found that the CO does not bind directly on top of the lead atom, as the binding energy is not significant compared to the binding energy of CO on Cu and CO on Au. During the optimisation the CO molecule moved away from the surface, the final distance is too big for a chemical bond between the CO and the surface. The optimization for Pb(111) with CO directly on top was started with the C atom at a distance of 0.150 nm from the surface. The DFT calculations show that the CO is binding on an site between atoms for Pb(111). Both for the two-fold hollow site and the three-fold hollow site there is a binding energy found comparable with CO on Cu(111) and CO on Au(111). The absolute value for CO on Cu(111) is bigger than the calculated value. The absolute values can differ from the ones calculated here because of multiple reasons. E.g. the restriction that the atoms of the surface do not move at all changes the energy, the type of exchange-correlation functional used changes the energy and the type of basis set used changes the energy. For the CO at the two-fold hollow site or three-fold hollow site the size of the crystal has to be taken into account. The size is quite small which can also effect the change in total energy. Also there are two kind of three-fold hollow sites, one for which there is a lead atom directly beneath it in the second layer (used here) and one were there is no lead atom directly beneath it in the second layer.

In figure 18 the change in electron density CO on Au(111) and CO on Cu(111) is shown, blue is a positive change, red is a negative change. The isovalue used was 0.002 electrons/Bohr^3. The change in electron density for CO directly above Pb(111)(not plotted here) was so small that is only can be seen with a isovalue of 0.0002 electrons/Bohr^3, this also shows that the CO does not bond directly on top of a Pb atom. For the configurations with CO between two lead atoms and between three lead atoms the results are shown in figure 19. For the latter Pb-CO clusters, the charge redistribution is larger than for the Au-CO and Cu-CO clusters. This suggests that the bond between the CO and Pb is stronger than between CO and the other two metals.

Type	Distance C from surface	Distance O from surface	Change in total energy	experimental value adsorption energy
Cu(111)	0.192 nm	0.307 nm	−0.30 eV	0.490 ± 0.015 eV[25]
Au(111)	0.210 nm	0.323 nm	−0.27 eV	
Pb(111) on top	0.384 nm	0.498 nm	−0.06 eV	
Pb(111) three-fold hollow	0.154 nm	0.273 nm	−0.24 eV	
Pb(111) two-fold hollow	0.178 nm	0.295 nm	−0.32 eV	

Table 1: DFT results for change in total energy and geometry optimization with ORCA[22] for CO on Cu(111), Au(111) and Pb(111). For CO on Cu(111) also the experimental value of the adsorption energy is given.

The change in the Pb crystals is not as symmetric as the change in the Au and Cu crystals. This can be due the smaller size of the surface. The change around the CO molecule looks the same for all crystals. A positive (blue) change (a higher electrons density) can be seen around the O atom and on the top of the C atom, with a negative change between the O and C atom. At the bottom of the C atom a negative change can be seen. For all atoms is the change below the CO at the surface negative.

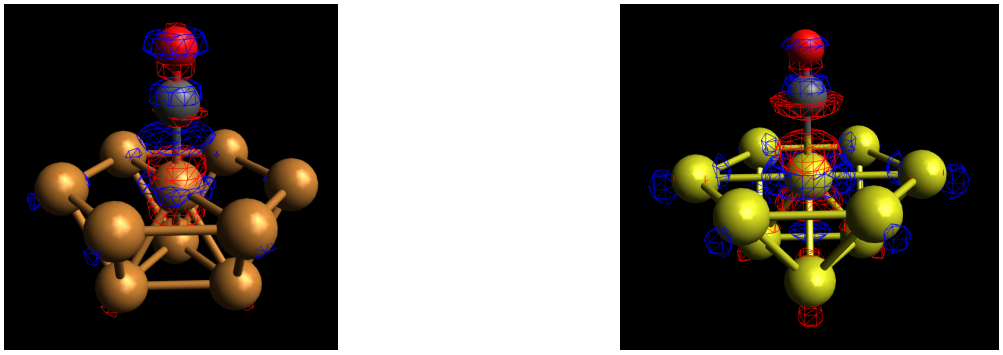

(a) (b)

Figure 18: Plot of change in electron density calculated with ORCA[22] due to binding of CO above (a) an Cu(111) surface (b) Au(111) surface . Plotted with Avogadro[23]. Blue is positive change, red is negative change. Isovalue=0.002 electrons/Bohr^3.

(a) (b)

Figure 19: Plot of change in electron density calculated with ORCA[22] due to binding of CO on (a) the two-fold hollow site of a Pb(111) surface (b) the three-fold hollow site of Pb(111) surface. Plotted with Avogadro[23]. Blue is positive change, red is negative change. Isovalue=0.002 electron/Bohr^3.

5 Conclusion

An atomically flat Pb(111) and Pb(100) surface under the STM has not yet been achieved. Sputtering and annealing changed the shape of the surface from small dome shaped height differences to height differences on a larger scale. In the future an option one has is annealing the sample to a higher temperature and sputtering more cycles with a more focused profile.
The DFT calculations showed that for Pb(111) the CO does not attach right above a Pb atom of the surface as is the case for CO on Au(111) and Cu(111). The binding energies for CO at the three-fold hollow site and two-fold hollow site were in the same range as CO on gold and copper. This suggests that it would be possible to manipulate CO molecules on Pb surfaces. More calculations have to be done with less constraints and larger parts of the crystal to properly compare the binding energy of CO on Pb(111) with CO on Cu(111) and Au(111) and make a prediction about CO manipulation on Pb(111).

6 Acknowledgements

I want to thank several people who helped me with this thesis. First I want to thank my daily supervisor Saoirsé Freeney for working with me and answering all my questions. I really enjoyed working together. I want to thank my supervisor Ingmar Swart, especially for the help with the DFT calculations. I want to thank Marlou Slot for helping me with the gold and explaining a lot about the STM microscope. I want to thank Marlou Slot and Nadine van der Heijden for the help with the lead samples. Finally I want to thank Utrecht University, the Debye Institute and the group of CMI for giving this opportunity to me.

A Preparation Pb(111)

Step	Time	Resistive Current(temperature)	Argon pressure	Comments
Sputtering	60 min	0A	6×10^{-6} mbar	
Sputtering (warm)	5 min	2A	6×10^{-6} mbar	
Sputtering	30 min	0A	6×10^{-6} mbar	
Sputtering	overnight	0A	begin: 3.2×10^{-6} mbar end:2.6×10^{-10} mbar	Energy: 5Kv Extractor 4410V Focus 4143
Annealing	10 min	2A		
Sputtering (warm)	105 min	1.5A	3.6×10^{-6} mbar	
Annealing	5 min	2.2A		
Sputtering (warm)	60 min	1.5A	3.6×10^{-6} mbar	
Sputtering (cold)	60 min	0A	3.6×10^{-6} mbar	
Annealing	5 min	2.2A		
Sputtering (cold)	106 min	0A	4.8×10^{-6} mbar	
Annealing	10 min	2.2A		
Sputtering (cold)	75 min	0A	4.3×10^{-6} mbar	
Annealing	10 min	2.2A		
Sputtering (cold)	40 min	0A	4.2×10^{-6} mbar	
Annealing	10 min	2.2A		
Sputtering (cold)	120 min	0A	4.3×10^{-6} mbar	
Annealing	10 min	2.2A		
Annealing	10 min	2.2 A		
Sputtering (warm)	37 min	1.3A	3.2×10^{-6} mbar	
Sputtering (cold)	28	0A	3.2×10^{-6} mbar	
Annealing	7 min	2.3A		
Sputtering (cold)	69 min	0A	3.2×10^{-6} mbar	
Annealing	7 min	2.2 A		
Sputtering	?	0A	$(3-6) \times 10^{-6}$ mbar	
Annealing	10 min	2.2 A		
Sputtering	?	0A	$(3-6) \times 10^{-6}$ mbar	
Annealing	10 min	2.2 A		
Sputtering	?	0A	$(3-6) \times 10^{-6}$ mbar	
Annealing	10 min	2.2 A		
Sputtering	?	0A	$(3-6) \times 10^{-6}$ mbar	
Annealing	10 min	2.2 A		
Sputtering	?	0A	$(3-6) \times 10^{-6}$ mbar	
Annealing	10 min	2.2 A		
Sputtering	?	0A	$(3-6) \times 10^{-6}$ mbar	
Annealing	10 min	2.2 A		
Sputtering	?	0A	$(3-6) \times 10^{-6}$ mbar	
Annealing	10 min	2.2 A		
Sputtering	?	0A	$(3-6) \times 10^{-6}$ mbar	
Annealing	10 min	2.2 A		measurement Fermi: figure 11
Sputtering (warm)	60min	1.5A	$(3-6) \times 10^{-6}$ mbar	
Annealing	10 min	2.2A (started at 1.5A)		
Sputtering (warm)	60min	1.5A	$(3-6) \times 10^{-6}$ mbar	
Annealing	10 min	2.2A (started at 1.5A)		
Sputtering (warm)	60min	1.5A	$(3-6) \times 10^{-6}$ mbar	
Annealing	10 min	2.2A (started at 1.5A)		

Sputtering (warm)	60min	1.5A	$(3-6)\times10^{-6}$ mbar	
Annealing	10 min	2.2A (started at 1.5A)		
Sputtering (cold)	overnight		$(3-6)\times10^{-6}$ mbar	
Annealing	30 min	2.2A		
Sputtering (cold)	30 min		$(3-6)\times10^{-6}$ mbar	
Anneailng	5 min	2.2A		
Sputtering (cold)	?		$(3-6)\times10^{-6}$ mbar	
Annealing	10 min	2.2A		
Sputtering	Overnight		$(3-6)\times10^{-6}$ mbar	
Annealing	10	2.2 A		
Sputtering	?	0A	$(3-6)\times10^{-6}$ mbar	
Sputtering (warm)	30 min	1.5A		
Annealing	10 min	2.7 A		
Sputtering (warm)	30 min	1.5 A	$(3-6)\times10^{-6}$ mbar	
Annealing	10 min	2.7 A		
Sputtering (warm)	30 min	1.5 A	$(3-6)\times10^{-6}$ mbar	
Annealing	10 min	2.7 A		
Sputtering (warm)	30 min	1.5 A	$(3-6)\times10^{-6}$ mbar	
Annealing	10 min	2.7 A		
Sputtering (warm)	30 min	1.5 A	$(3-6)\times10^{-6}$ mbar	
Annealing	5 min	2.7 A		
Sputtering(warm)	60 min	1.5 A	$(3-6)\times10^{-6}$ mbar	
Annealing	10 min	2.7A		
Sputtering(warm) Annealing	60 min 10 min	1.5 A 2.2 A	$(3-6)\times10^{-6}$ mbar	

Table 2: Overview of all sputtering and annealing steps of the un-etched Pb(111), if there is a ? the precise time is unknown, but it is between one and several hours (less than a day).

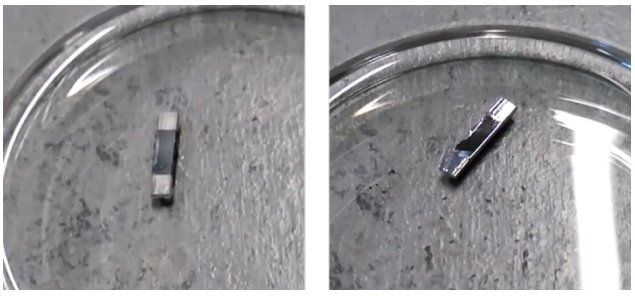

Figure 20: Pb(111) during etching. Left picture: Pb(111) before etching started. Right picture: Pb(111) after 5 minutes of etching.

Step	Time	Resistive Current(temperature)	Argon pressure	Comments
Annealing	9 min	1.7A		
Annealing	97 min	1.7A		measurement Fermi: figure 12
Sputtering(cold)	14 h	0A	begin:3.6×10^{-6} mbar end:4.2×10^{-6} mbar	
Annealing	5h 30 min	1.7A		
Sputtering(cold)	1h 59 min	0A	begin:4.2×10^{-6} mbar end:4.8×10^{-6} mbar	

Annealing	18h 40 min	1.7A		
Sputtering(cold)	2h 30 min	0A	3.6×10^{-6} mbar	
Annealing	6h 10min	1.7A		
Sputtering(warm)	1h 3min	1.0A	4.4×10^{-6} mbar	measurement Fermi: figure 13
Annealing	17h 20 min	1.8A		

Table 3: Overview of all sputtering and annealing steps of the etched Pb(111).

B Preparation Pb(100)

Figure 21: Picture of Pb(100) directly after etching.

Step	Time	Resistive Current(temperature)	Argon pressure	Comments
Sputtering(cold)	3h 17 min	0A	begin:4.0×10^{-6} mbar end:4.6×10^{-6} mbar	
Annealing	2h 23 min	1.7 A		
Sputtering(cold)	4h 8 min	0A	begin:3.9×10^{-6} mbar end:4.7×10^{-6} mbar	
Annealing	2h 3min	1.7A		measurement Fermi: figure 14
Sputtering(cold)	1h 1min	0A	3.9×10^{-6} mbar end:4.2×10^{-6} mbar	
Annealing	5h 24min	1.7A		
Sputtering (cold)	1h 1min	0A	begin:3.8×10^{-6} mbar end:4.2×10^{-6} mbar	
Annealing	1h 48 min	1.7A		
Sputtering (cold)	1h 10 min	0A	3.7×10^{-6} mbar	
Annealing	15h 50 min	1.7A		Picture of sample figure 22 measurement Fermi: figure 15 Measurement LT: figure 16

Table 4: Overview of all sputtering and annealing steps of the etched Pb(100).

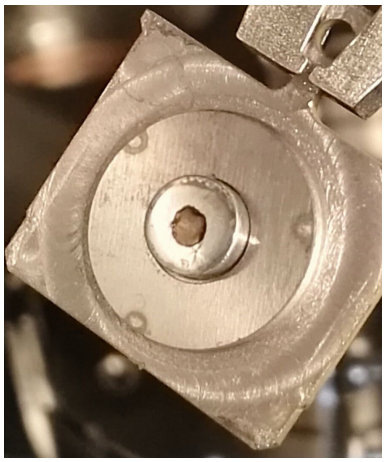

Figure 22: Picture of Pb(100) after all sputtering and annealing steps.

References

[1] K. K. Gomes, W. Mar, W. Ko, F. Guinea, and H. C. Manoharan, Nature **483**, 306 (2012).

[2] M. R. Slot, T. S. Gardenier, P. H. Jacobse, G. C. P. van Miert, S. N. Kempkes, S. J. M. Zevenhuizen, C. Morais Smith, D. Vanmaekelbergh, and I. Swart, ArXiv e-prints (2016), 1611.04641.

[3] M. Ruby, B. W. Heinrich, J. I. Pascual, and K. J. Franke, Phys. Rev. Lett. **114**, 157001 (2015), URL http://link.aps.org/doi/10.1103/PhysRevLett.114.157001.

[4] S. Speller, W. Heiland, A. Biedermann, E. Platzgummer, C. Nagl, M. Schmid, and P. Varga, Surface science **331**, 1056 (1995).

[5] B. Voigtländer, *Scanning probe microscopy: Atomic force microscopy and scanning tunneling microscopy* (Springer, 2015).

[6] C. J. Chen and W. F. Smith, American Journal of Physics **62**, 573 (1994).

[7] C. Kittel, *Introduction to Solid State Physics* (Wiley, 2005), 8th ed., ISBN 047141526X.

[8] S. Crampin, M. H. Boon, and J. E. Inglesfield, Phys. Rev. Lett. **73**, 1015 (1994), URL https://link.aps.org/doi/10.1103/PhysRevLett.73.1015.

[9] H. H. J.R.Hook, *Solid State Physics* (Wiley, 1991), 2nd ed., ISBN 0471928054.

[10] L. Bartels, G. Meyer, and K.-H. Rieder, Phys. Rev. Lett. **79**, 697 (1997), URL http://link.aps.org/doi/10.1103/PhysRevLett.79.697.

[11] R. J. Celotta, S. B. Balakirsky, A. P. Fein, F. M. Hess, G. M. Rutter, and J. A. Stroscio, Review of Scientific Instruments **85**, 121301 (2014).

[12] L. Bartels, G. Meyer, K.-H. Rieder, D. Velic, E. Knoesel, A. Hotzel, M. Wolf, and G. Ertl, Phys. Rev. Lett. **80**, 2004 (1998), URL https://link.aps.org/doi/10.1103/PhysRevLett.80.2004.

[13] L. Bartels, G. Meyer, and K.-H. Rieder, Applied physics letters **71**, 213 (1997).

[14] J. Barth, H. Brune, G. Ertl, and R. Behm, Physical Review B **42**, 9307 (1990).

[15] C. J. Murphy, X. Shi, A. D. Jewell, A. F. McGuire, D. O. Bellisario, A. E. Baber, H. L. Tierney, E. A. Lewis, D. S. Sholl, and E. C. H. Sykes, The Journal of chemical physics **142**, 101915 (2015).

[16] P. Hohenberg and W. Kohn, Physical review **136**, B864 (1964).

[17] M. C. H. Wolfram Koch, *A Chemist's Guide to Density Functional Theory* (Wiley–VCH Verlag, 2001), 2nd ed., ISBN 3527600043.

[18] L. Kuipers, M. S. Hoogeman, J. W. M. Frenken, and H. van Beijeren, Phys. Rev. B **52**, 11387 (1995), URL http://link.aps.org/doi/10.1103/PhysRevB.52.11387.

[19] L. Kuipers and J. W. M. Frenken, Phys. Rev. Lett. **70**, 3907 (1993), URL http://link.aps.org/doi/10.1103/PhysRevLett.70.3907.

[20] R. Joyner, K. Kishi, and M. Roberts, in *Proceedings of the Royal Society of London A: Mathematical, Physical and Engineering Sciences* (The Royal Society, 1978), vol. 358, pp. 223–241.

[21] S. Kandoi, A. Gokhale, L. Grabow, J. Dumesic, and M. Mavrikakis, Catalysis Letters **93**, 93 (2004).

[22] F. Neese, Wiley Interdisciplinary Reviews: Computational Molecular Science **2**, 73 (2012).

[23] M. D. Hanwell, D. E. Curtis, D. C. Lonie, T. Vandermeersch, E. Zurek, and G. R. Hutchison, Journal of cheminformatics **4**, 17 (2012).

[24] *Lattice constants of the elements*, http://periodictable.com/Properties/A/LatticeConstants.html, accessed: 2017-06-30.

[25] S. Vollmer, G. Witte, and C. Wöll, Catalysis letters **77**, 97 (2001).